J Food Sci Technol (October 2023) 60(10):2659–2669
https://doi.org/10.1007/s13197-023-05790-4

ORIGINAL ARTICLE

Tannic acid-layered hydroxide salt hybrid: assessment of antibiofilm formation and foodborne pathogen growth inhibition

Dulce María Romero-García[1] · Carlos Arnulfo Velázquez-Carriles[2] · Cesar Gomez[1] · Gilberto Velázquez-Juárez[3] · Jorge Manuel Silva-Jara[2]

Revised: 10 April 2023 / Accepted: 6 June 2023 / Published online: 7 July 2023

Abstract Pathogenic bacteria in food are a public health problem worldwide. Polyphenolic bioactive compounds with antimicrobial activity and antioxidant capacity represent a tangible alternative to overcome this problem. To preserve the biological functions of phenolic compounds such as tannic acid, which has been described to possess antioxidant and antimicrobial activity, this study describes the synthesis of a zinc nanohydroxide to stabilize its properties. Characterization by XRD, FT-IR, SEM, DLS, and UV-vis evidenced the presence of tannic acid in the nanohybrid TA-Zn-LHS which was further confirmed by DPPH, ABTS and FRAP antioxidant activity techniques. Bacterial growth inhibition of *Escherichia coli* ATCC 8739, *Salmonella* Enteritidis, and *Staphylococcus aureus* ATCC 25923 was over 80% at 50 mg/mL of the TA-Zn-LHS and over 90% with Zn-LHS. Antibiofilm evaluation of these same strains showed biofilm formation inhibition > 90% and > 80% for Zn-LHS and TA-Zn-LHS, respectively. The toxicity evaluation of the materials in *Artemia salina* showed a classification of the materials as non-toxic to slightly toxic in concentrations up to 1 mg/mL. These results allow us to introduce a new nanohybrid useful for food safety with safe biological functions.

Keywords Tannic acid · Nanohybrid · Layered hydroxide salt · Antibiofilm activity · Antimicrobial compound · Antioxidant activity

✉ Jorge Manuel Silva-Jara
jorge.silva@academicos.udg.mx

[1] Chemical Engineering Department, Universidad de Guadalajara CUCEI, Guadalajara, Jalisco 44430, México

[2] Pharmacobiology Department, Universidad de Guadalajara CUCEI, Guadalajara, Jalisco 44430, México

[3] Chemistry Department, Universidad de Guadalajara CUCEI, Guadalajara, Jalisco 44430, México

Abbreviations

ABTS	2,2′-Azino-bis(3-ethylbenzothiazoline-6-sulfonate)
DLS	Dynamic light scattering
DPPH	2,2 Diphenyl-1-picrylhydrazyl
FRAP	Ferric reducing antioxidant power
FT-IR	Fourier transform infrared spectroscopy
LHS	Layered hydroxide salt
OD	Optical density
SEM	Scanning electron microscopy
TA	Tannic acid
XRD	X-ray diffraction

Introduction

Foodborne diseases are considered a public health problem worldwide, causing ailments ranging from nausea, headache, diarrhea, and vomiting to death in affected individuals. These symptoms are derived from the consumption of food and water contaminated by different microorganisms (bacteria, viruses, parasites, or fungi), as well as chemical substances (i. e. heavy metals) (World Health Organization 2015). Food contamination can occur at any stage of the food production, delivery, and consumption chain. New technologies with antimicrobial capacity based on physical, chemical, and biological strategies have been developed (Sánchez-Maldonado et al. 2018). Polyphenolic compounds are used as antioxidants, additionally they impart or enhance nutritional properties, biological and antimicrobial effects, and sensory attributes.

Tannic acid (TA) is a polyphenolic compound of the tannin group that possesses functional properties such as antimicrobial activity against Gram-positive and Gram-negative bacteria, including *Escherichia coli, Staphylococcus aureus*

and *Pseudomonas aeruginosa* (Kaczmarek 2020). The use of TA-hydrogels and TA-ferromagnetic and silver nanoparticles, mainly for biomedical purposes has been previously explored (Santos et al. 2016). Its application is related to functional properties such as antioxidant, antimicrobial, anti-inflammatory and antitumor activity. Despite possessing biological functions of health interest, this type of polyphenolic compound presents limiting factors for its application, such as low stability in oxygenated environments, sensitivity to light and temperature, low solubility, and limited bioavailability (Rezaei et al. 2019). An alternative to overcome these limitations is to intercalate these compounds into layered hydroxide salts (LHS) conferring them stability and protection while maintaining or enhancing their bioactive functional properties.

LHS are two-dimensional (2D) compounds also known as anionic clays, whose structure is maintained by weak bonds such as van der Waals or electrostatic forces (Carbajal-Arízaga et al. 2007). They possess excellent ion exchange capacity, which allows them to intercalate other chemical compounds (Nakagaki et al. 2021).These nanohydroxides are materials whose composition is based on the general formula $[M^{2+}(OH)_{2-x}(A^{m-})_{x/m} \bullet nH_2O]$, where M^{2+} represents a divalent cation such as Mg^{2+}, Zn^{2+}, Ni^{2+}, Ca^{2+}, Cd^{2+}, Co^{2+}, Cu^{2+}, among others; and A^{m-} represents intercalated anions (CO_3^{2-}, Cl^- or Br^-). LHS have a structure based on modifying layered magnesium hydroxide [$Mg(OH)_2$], known as brucite. In such modification, the structural hydroxyl groups can be replaced by anionic compounds or water, leading to the formation of a hydroxisalt. The synthesis of these compounds can be carried out using a metal salt precipitation methodology, using alkaline solutions, such as sodium hydroxide (NaOH) (Carbajal-Arízaga et al. 2007).

This study aimed to propose a zinc-LHS as a suitable matrix for the incorporation of tannic acid contemplating LHS properties to immobilize bioactive compounds in its structure. Likewise, the synthesis is considered a simple process carried out in short-time periods with low-cost materials, allowing it to be easily commercialized. TA-Zn-LHS aimed to protect and stabilize antioxidant capacity and, at the same time, maintain antimicrobial and antibiofilm activity of bioactive compound against foodborne pathogens.

Materials and methods

Synthesis of Zn-LHS and TA immobilization

The synthesis of Zn-LHS was carried out by modifications to the precipitation method reported by Velázquez-Carriles et al. (2020). For this purpose, 200 mL of 0.04 g $ZnCl_2$ / mL distilled water, was prepared under constant stirring. Once the $ZnCl_2$ was dissolved and maintained the agitation, 3 M NaOH was added dropwise as precipitant. The volume of NaOH consumed to reach a pH of 8.0 was recorded (HANNA potentiometer, model HI98115), and the solution was kept in agitation for 24 more h at room temperature for stabilization. The final precipitation product was centrifuged (LZ-1580R, LaboGene) at 11424 × g for 10 min at 25 °C. Two washes with 200 mL distilled water were performed under the same centrifugation conditions. The Zn-LHS precipitate was oven dried at 45 °C for 24–48 h, ground in an agate mortar, and stored. For the synthesis of the nanohybrid, a 50 mL solution of 5 mg/mL tannic acid (Sigma Aldrich, St. Louis, MO, USA) was prepared, and under constant stirring, 500 mg of dried Zn-LHS were added in the TA solution. The absorbance was continuously quantified in a spectrophotometer (NanoDrop™2000, Thermo Scientific™) at 325 nm until a steady decrease was observed. The TA-Zn-LHS synthesized was then dried at 45 °C for 24 h, ground in an agate mortar, and stored at room temperature.

Characterization of zinc nanohydroxides

Powder X-ray diffraction (XRD)

X-Ray Diffraction (XRD) analysis was carried out to determine the structural composition of the synthesized layered hydroxide salt and the nanohybrid. The analysis was performed on an X-Ray diffractometer (Malvern Panalytical Empyrean, UK) with CuKα radiation with a 2θ angle from 5° to 70° with a step of 0.02 and a collection time of 30 s per step.

Fourier Transform infrared spectroscopy (FT-IR)

Fourier-transform infrared spectroscopy (FT-IR) analysis was performed to obtain the absorption spectrum and identify the presence of functional groups. FT-IR spectra were collected in the range 4000–400 cm^{-1} in absorbance mode at 32 scans and 4 cm^{-1} resolution, using an FT-IR spectrophotometer with an attenuated total reflectance (ATR) device (Cary 630, Agilent Technologies, inc, CA, USA).

Scanning electron microscopy (SEM)

The surface morphology of the nanohydroxides was determined by Scanning Electron Microscopy (SEM) to obtain high-resolution images of the materials. Zn-LHS and TA-Zn-LHS were placed in pin stub sample holders and coated with a thin layer of gold for 20 s. Scanning electron microscopy was carried out on a field emission scanning electron microscope (FE-SEM, TESCAN, model MIRA 3 LMU, Brno, Czech Republic) with an accelerating potential of 15 kV.

Dynamic light scattering (DLS)

The particle-size, polydispersity index (PDI) and zeta potential (ζ) of the materials were determined by the dynamic light scattering (DLS) technique, using a Zetasizer Nano equipment (Malvern Instruments, UK). 1 mg of each of the materials was dissolved in distilled water and sonicated for 10 min (in 2 intervals of 5 min), at 25 °C. Serial dilutions of each of the material were performed to determine the particle size in four-sided polystyrene cells. Zeta potential quantification was carried out at 25 °C in polystyrene cells. Measurements were determined by performing 20 runs in triplicate with stabilization intervals every 5 s.

Spectrophotometry UV-Vis

The adsorption of tannic acid in the Zn-LHS was evaluated during the synthesis procedure. The amount of adsorbed compound was determined according to Bouaziz et al. (2018):

$$\Gamma_e = \left(C_0 - C_e\right)\frac{v}{m}$$

where Γ_e is the interfacial concentration of tannic acid (TA mg/ Zn-LHS mg), C_0 is the initial concentration of tannic acid (TA mg/mL). C_e is the supernatant concentration of tannic acid (TA mg/mL). v is the volume of the suspension in mL and m is the mass of LHS in mg.

Antimicrobial activity

Bacterial inoculum

Escherichia coli ATCC 8739, *Salmonella Enteritidis* (isolated and sequenced from a clinical case of salmonellosis, kindly donated by the molecular biology laboratory, Universidad de Guadalajara, JAL, MEX), and *S. aureus* ATCC 25923 were cultured on nutrient slant agar and incubated at 37 °C for 24 h. The concentration of bacteria was adjusted by optical density (OD) by measuring the absorbance at 600 nm in a UV–Vis spectrum (OPTIZEN Pop, K LAB) according to the Mexican Standard NMX-BB-040-SCFI-1999 for the determination of antimicrobial activity in germicidal products. Serial dilutions were performed in phosphate buffered solution (PBS).

Microdilution plate method

The microdilution plate method was performed using a 96-well microplate in which 160 µL of TSB (trypticase soy broth) culture medium was placed into the well, then 20 µL of bacterial inoculum (1X10^6 CFU/mL) were added, and 20 µL of 50 mg TA-Zn-LHS/ mL PBS) as a treatment. Culture medium with PBS as a negative control were also evaluated. Ampicillin (0.1 mg/mL) was used as a positive control. Microplates were incubated for 24 h at 37 °C and microplate measurement was performed in a 96-well plate reader (BioRad, iMark™, CA, USA) at a wavelength of 600 nm. The bacterial growth inhibition rate (BGIR) percentage was determined according to Balouiri et al. (2016):

$$\text{BGIR}\ (\%) = \left(\frac{\left(\text{OD}_{(-)\text{control}} - \text{OD}_{\text{treatment}}\right)}{\text{OD}_{(-)\text{control}}}\right) * 100$$

where de $\text{OD}_{(\text{-})\text{control}}$ is the OD of the strain inoculum at 24 h of bacterial growth (BG); $\text{OD}_{\text{treatment}}$ corresponds to the OD of the strain inoculum after the treatment with the Zn-LHS or the TA-Zn-LHS.

Antibiofilm activity

Microplate antibiofilm formation assay was performed according to O'Toole (2011) were *P. aeruginosa* was evaluated, with modifications. This trial assessed the antibiofilm capacity of Zn-LHS and TA-Zn-LHS against the bacterial strains mentioned above. The initial inoculum (1×10^9 CFU/mL) was diluted 1:100 in fresh medium for the assay. 100 µL of the diluted culture was placed in a 96-well microplate in triplicate for each treatment with 20 µL of 50 mg nanohydroxides/mL PBS. The microplate was incubated for 4–24 h at 37 °C. After the incubation period, the liquid was discarded by decanting. Then, two washes were performed by immersion in distilled water, the formed biofilm was stained with 125 µL of 0.1% crystal violet (CV) in each well of the microplate and incubated at room temperature for 15 min. After incubation, the CV solution was removed, and four washes were performed with distilled water. Excess water was removed by striking the inverted plate on a paper towel. The plate was left to dry overnight and then the biofilm quantification was carried out.

To quantify biofilm formation, 125 µL of 30% acetic acid was added to each microplate well to solubilize the stained biofilm. The microplate was incubated at room temperature for 10–15 min. After the incubation time, the 125 µL of the stained biofilm was transferred into a new clean microplate to quantify its absorbance in a microplate reader (BioRad, iMark™, CA, USA) at 550 nm, using 30% acetic acid as blank. The following equation determined the biofilm inhibition (BFI) percentage (O'Toole 2011):

$$\text{Biofilm inhibition}\ (\%) = \left[1 - \frac{\left(\text{Abs}_{\text{sample}} - \text{Abs}_{\text{blank}}\right)}{\left(\text{Abs}_{\text{control}} - \text{Abs}_{\text{blank}}\right)}\right] * 100$$

where $\text{Abs}_{\text{sample}}$ is the absorbance of the that contains all the reagents including the Zn-LHS or the TA-Zn-LHS. $\text{Abs}_{\text{control}}$

is the absorbance of control with all the reagents, except the nanohydroxides.

Antioxidant activity

DPPH

Antioxidant activity was evaluated by the 2,2-diphenyl-1-picrylhydrazyl radical (DPPH) scavenging capacity technique according to the methodology described by Brand-Williams et al. (1995) with the following modifications adapted for microplate. The 0.04% (w/v) DPPH reagent in methanol was prepared as a working solution and protected from light. Two calibration curves were constructed, Trolox (6-hydroxy-2,5,7,8-tetramethylchroman-2-carboxylic acid, 0–1280 µg/mL) and TA (0–40 µg/mL). The measurement was performed in a 96-well microplate in quadruplicate, adding 20 µL of the sample (1 mg LHS/ mL distilled water) and 280 µL of the 0.04% DPPH reagent. Methanol was used as a blank. The samples were incubated at room temperature, in the dark, for 30 min, subsequently measuring the absorbance at 515 nm in a microplate reader equipped with the software SkanIt (Multiskan SkyHigh; SkanIt software 6.0.1 ver. 6.0.1.6, ThermoFisher Scientific MA, USA). The result of DPPH is presented as µM equivalent of TA.

ABTS

The 2,2'-azino-bis(3-ethylbenzothiazoline-6-sulfonate) (ABTS) radical scavenging activity was performed with modifications for microplate, according to Li et al. (2009). A stock solution of 7 mM ABTS radical in distilled water was prepared, and subsequently, 4 mM ammonium persulfate (in distilled water) was added in equal amounts. The solutions were allowed to react for 12–16 h at 4 °C in the dark. The absorbance of the ABTS stock was adjusted to 0.7 ± 0.05 at 750 nm (Multiskan SkyHigh, ThermoFisher Scientific, MA, USA) with distilled water. Trolox (0–400 µg/mL) and TA (0–40 µg/mL) were used as positive controls, and calibrations curves were performed for each one. In a 96-well microplate, 280 µL of stock solution and 20 µL of the materials were placed, quadruplicate. Measurements were performed by incubating in the dark for 30 min and monitoring the reaction at 750 nm in a microplate reader. The result of ABTS is presented as µM equivalents of TA.

FRAP

The determination of ferric reducing antioxidant power (FRAP) was performed as Benzie and Strain (1996) reported with modifications adapted to 96-well microplate. FRAP working solution was prepared to contain: 2.5 mL of 20 mM ferric chloride ($FeCl_3$), 2.5 mL of 2,4,6-tripyridyl-S-triazine (TPTZ) 10 mM in 40 mM hydrochloric acid (HCl), and 25 mL of 0.3 mM sodium acetate buffer, pH 3.6. Trolox (0–400 µg/mL) and tannic acid (0–50 µg/mL) were used as positive controls, and calibrations curves were performed for each one. In a 96-well microplate, 40 µL of the sample (1 mg LHS/mL distilled water), 40 µL of acetate buffer, and 150 µL of working solution were placed. Samples were incubated in the dark at 37 °C for 30 min. Measurements were performed, quadruplicate, and absorbance was measured at 595 nm in a microplate reader (Multiskan SkyHigh, ThermoFisher Scientific, MA, USA). The result of FRAP is presented as µM equivalents of TA.

Artemia salina toxicity bioassay

The degree of toxicity of hybrid and non-hybrid hydroxides was evaluated using the *A. salina* bioassay. Brine shrimp cysts were incubated at 28 °C in synthetic seawater (30 g/L) for 24 h under continuous light and aeration. Ten nauplii of *A. salina* (Fish & Animals, JAL, MEX) were added per well to a 6-well cell culture plate and brought to a volume of 5 mL with artificial seawater using the nanohydroxide materials as treatment. Dimethyl sulfoxide was used as a positive control. Nauplii were counted with the aid of a light camera for contrast. The nauplii were kept in darkness, and the percentage of deaths at 24 h was counted at each of the concentrations of tannic acid, Zn-LHS and TA-Zn-LHS. The percentage of deaths was determined as follows (Casas-Junco et al. 2019):

$$\text{Mortality}(\%) = \frac{\text{Dead nauplii in the bioassay}}{\text{Nauplii used in the bioassay} - \text{Dead nauplii in the control}} * 100$$

Toxicity was established according to mortality percentage: 0–9% = non-toxic (NT); 10–49% = slightly toxic (ST); 50–89% = toxic (T); 90–100% = very toxic.

Statistical analysis

All tests and measurements were carried out in at least triplicate, and the results were analyzed by one-way analysis of variance (ANOVA). Results are presented as mean ± standard deviation (SD), being established statistical significance at p-value < 0.05. Statistical analysis was performed using Statgraphics Centurion 19® (Statgraphics Technologies, Inc. VA, USA).

Results and discussion

XRD, FT-IR SEM and DLS analysis

The results shown below correspond to the structural, morphological, and hydrodynamic characteristics of Zn-LHS and TA-Zn-LHS. Figure 1 summarizes the characterization results of the Zn-LHS and TA nanohybrid according to XRD patterns, FT-IR spectra, and SEM micrographs. The XRD pattern (Fig. 1a) shows that in both Zn-LHS and TA-Zn-LHS, the characteristic reflections for $Zn_5(OH)_8Cl_2•H_2O$ were observed, with the basal reflection of highest intensity at 11.29° of the 2θ angle (ICDDD No. 07-0155). This reflection represents the interlaminar distance of the hydroxisalt, its value 7.83 Å, according to Bragg's law. In the case of the Zn-LHS and TA-Zn-LHS, the interlaminar spacing distance obtained was 7.83 and 7.90 Å, respectively. By not observing a shift in the basal reflections of the diffraction pattern for TA-Zn-LHS compared to Zn-LHS, it could be assumed that TA intercalation did not occur. However, TA-Zn-LHS shows a lower intensity in some reflections, indicating a loss of crystallinity, possibly due to the partial presence of TA on the nanohydroxide surface. Bouaziz et al. (2018), obtained this same effect by synthesizing Zn/Al (Cl^-)-Layered Double Hydroxides (LDH) hybrid materials with tetracycline and oxytetracycline. The authors found the same basal pattern in the LDH with and without antibiotics. However, they described a decrease in the intensity of the diffraction signals

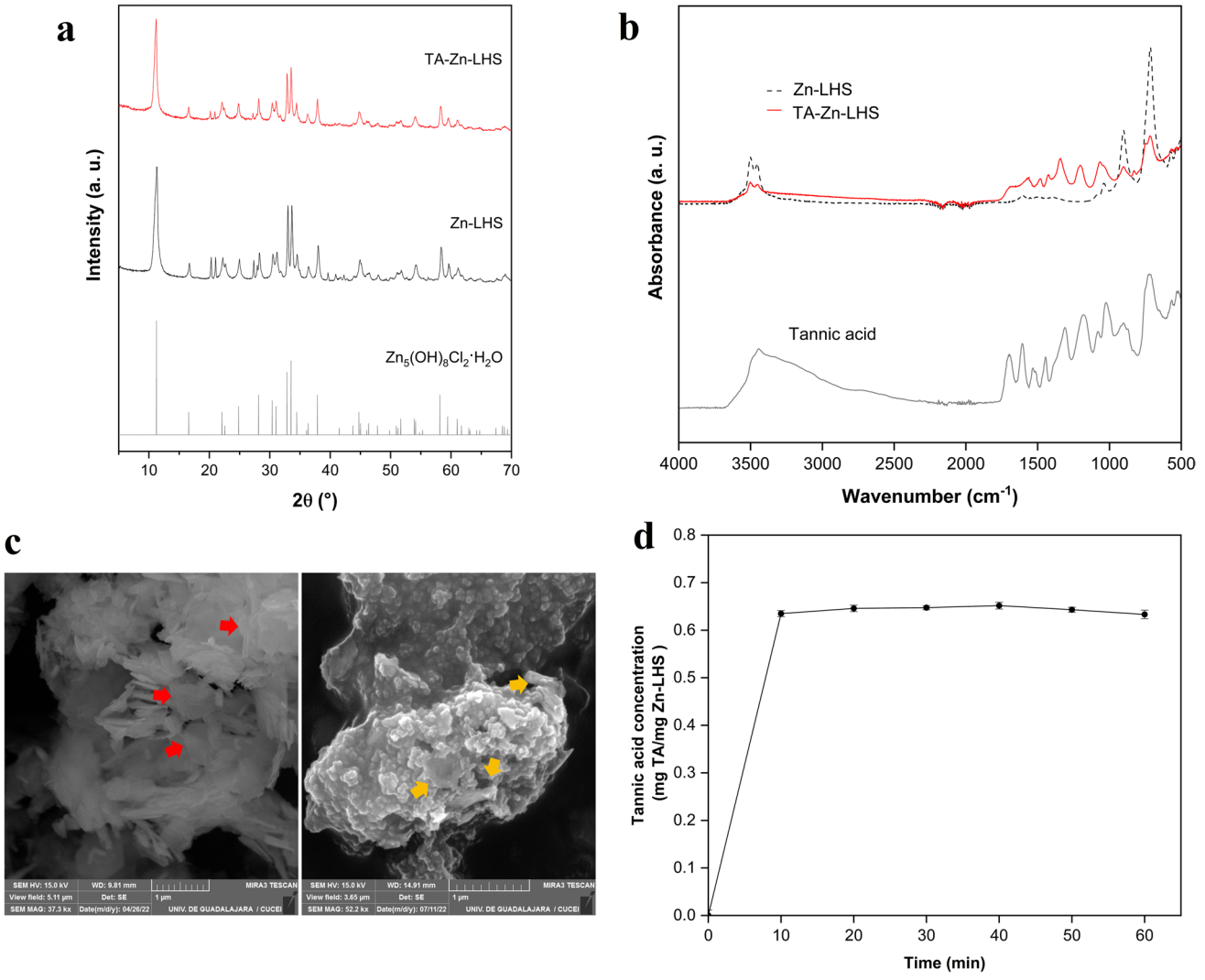

Fig. 1 Characterization of Zn-LHS and TA-Zn-LHS: **a** Diffractogram of $Zn_5(OH)_8Cl_2•H_2O$ (gray line), Zn-LHS (black line) and TA-Zn-LHS (red line); **b** infrared spectra of Zn-LHS (black dashed line), TA-Zn-LHS (red solid line) and tannic acid (gray solid line); Scanning electron micrographs of **c** Left: Zn-LHS, SEM magnification: 37.3 kx, and Right: TA-Zn-LHS, SEM magnification: 52.2 kx; **d** Tannic acid adsorbed concentration in Zn-LHS (Color figure online)

caused by the presence of the antibiotics on the external surface of the Zn/Al-LDH synthesized by different methods.

In the FT-IR spectra (Fig. 1b) a doublet is observed in the 3500–3400 cm^{-1} region, the band positioned towards 3440 cm^{-1} is attributed to intermolecular couplings of inter-associative or interlaminar OH vibrations (Mohsin et al. 2013); this fact is also resolved, in the vicinity of 1015–755 cm^{-1}, the result of which is Zn-OH bending and OH torsional vibrations (peak around 897 cm^{-1}) (Sirvastava and Secco 1967). Also, the regions from 855 to 790 cm^{-1} are attributed to out-of-plane vibrations of ZnOHCl (a weak signal appearing only in the spectrum of the TA-Zn-LHS). In this sense, the inductive effect of chlorine may contribute to the decrease on peak high at 897 cm^{-1} for TA-Zn-LHS and the appearance of a weak signal at 827 cm^{-1}. A considerable decrease in signal strength is observed around 3500 cm^{-1} for TA-Zn-LHS. This fact warns of the strong interaction of the biomolecule as in the studies published by Velázquez-Carriles et al. (2020), where they observed this same phenomenon for nisin and simonkolleite. Due to the presence of tannic acid the majority of adsorption through hydrogen bonds present in the inorganic matrix its suggested.

For the hybrid compound, a signal appears at 744 cm^{-1} which is due to the presence of TA. Bands attributed to this aromatic nature appear around 1700 cm^{-1}, which in the spectrum of the TA-Zn-LHS shows the presence of this C=O vibration. Signals between 1300 and 1050 cm^{-1} are attributed to the C–O vibration belonging to aromatic esters (symmetrical and asymmetrical tension vibrations) (Wahyono et al. 2019). For the TA spectrum, the position appears specifically at 1177 cm^{-1}. In contrast, the nanohybrid shifts to higher energy levels around 1206 cm^{-1}, with a shift of $\Delta v = 29$ cm^{-1}.

The morphology and crystallinity of the hydroxisalt are of practical importance, compounds with biological activity are easily incorporated into the matrix, and changes to the initial structure are readily observed (Velázquez-Carriles et al. 2020). SEM micrographs showed a hexagonal morphology (red arrows on Fig. 1c, left) characteristic of Zn-LHS. In the case of TA-Zn-LHS (Fig. 1c, right) an amorphous agglomeration is observed surrounding the surface of the zinc sheets (yellow arrows) conferring a rough appearance to the crystalline surface thus indicating the presence of TA on the surface of the hydroxisalt.

The hydrodynamic behavior of the nanohydroxides was characterized by DLS (Table 1). The mean particle size of Zn-LHS was 489.3 nm being statistically different ($p < 0.05$) from TA-Zn-LHS with 550.3 nm. The PDI provides information regarding the degree of uniformity in the size distribution of a sample ranging from 0 to 1 (dimensionless), where a PDI close to 0 indicates the presence of a monodisperse sample. Whereas a PDI close to 1 represents a polydisperse sample, i.e., with a wide variety of sizes (Lancheros et al. 2014). The PDI of Zn-LHS and TA-Zn-LHS were large, 0.443 and 0.513, respectively but not statistically different ($p < 0.05$), suggesting a polydisperse suspension. The stability of the layered hydroxides mixture was determined by ζ, which indicates the stability of particles in a solution. High values of ζ (± 30 mV) indicate high colloidal stability (Orlowski et al. 2018). The ζ for Zn-LHS was 41.43 mV, upon incorporation of tannic acid, the ζ change to a negative value of − 21.13 mV, considered to be a colloidal material with moderate stability. The change in the zeta potential can be attributed to the presence of tannic acid since hybrid materials with polyphenolic compounds possess favorable dispersion characteristics in aqueous media and improve their stability. Specifically, the presence of TA has presented this same behavior in ferromagnetic hybrid nanoparticles, increasing their zeta potential. Due to the negative charge provided by the adsorption of TA on the surface of the materials and its molecular size, it is possible to attribute an enhancement in the aggregation phenomenon, as well as electrostatic repulsion (Santos et al. 2016).

Table 1 Characterization parameters determined by DLS for Zn-LHS and TA-Zn-LHS

Material	Particle size (nm)	PDI	ζ (mV)
Zn-LHS	489.3 ± 21.91[a]	0.443 ± 0.094[a]	41.43 ± 1.464[a]
TA-Zn-LHS	550.3 ± 3.42[b]	0.513 ± 0.035[a]	-21.13 ± 0.681[b]

PDI Polydispersity index, *ζ* Zeta potential. Mean ± standard deviation, n = 3. Different letters (by column) indicate significant differences according to Tukey's test ($p < 0.05$)

Adsorption of tannic acid in Zn-LHS

The incorporation of TA into Zn-LHS was determined with UV-vis at 325 nm. The adsorption of TA on top Zn-LHS its finished in 10 min and TA it's not released for at least 12 h (data not shown). The maximum concentration obtained was 0.643 ± 0.007 mg TA/ mg Zn-LHS, as shown in Fig. 1d. In the study conducted by Velázquez-Carriles et al. (2022), 0.863 mg thymol/mg Zn-LHS were adsorbed in 1.5 h. The results suggested that the adsorption of the bioactive compound was due to a small structure of the thymol on the zinc matrix, while in this research the lower concentration achieved could be as consequence of the complex structure of the tannic acid.

Antimicrobial and antibiofilm evaluation for *E. coli* ATCC 8739, *S.* Enteritidis and *S. aureus* ATCC 25923

The antimicrobial activity of Zn-LHS and TA-Zn-LHS against Gram-negative bacteria *E. coli* ATCC 8739 and

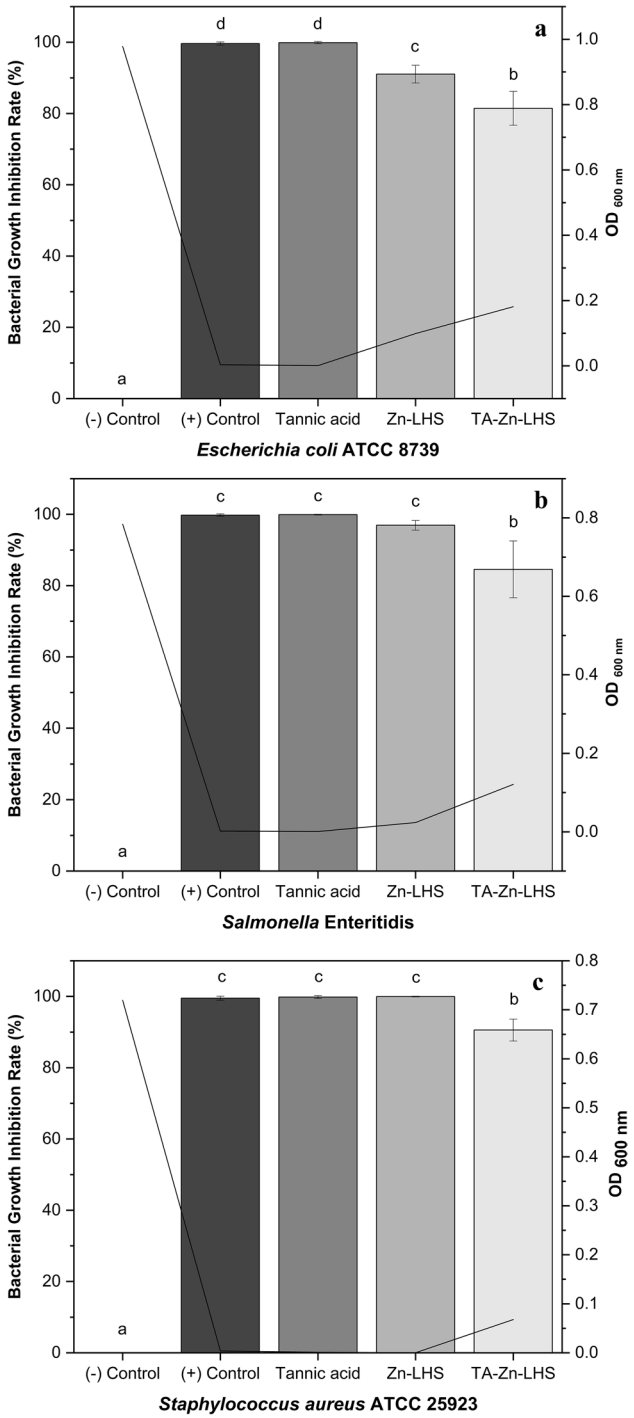

Fig. 2 Bacterial growth inhibition to: **a** *Escherichia coli* ATCC 8739; **b** *Salmonella* Enteritidis; **c** *Staphylococcus aureus* ATCC 25923. (−) Control: Strain inoculum; (+) Control: 0.1 mg/mL Ampicillin; OD: Optical Density. Different letters show statistical significance differences ($p < 0.05$) by Tukey's test

S. Enteritidis was above 90%. The BGIR was significantly lower in TA-Zn-LHS for *E. coli* ATCC 8739 (Fig. 2a) and *S.* Enteritidis (Fig. 2b) with 81.47 ± 4.75% and 84.56 ± 0.12%, respectively. For *S. aureus* ATCC 25923 (Fig. 2c), the BGIR was 99.95 ± 0.10% and 90.57 ± 3.08% for Zn-LHS and TA-Zn-LHS, respectively, finding no statistically significant differences ($p < 0.05$) with the positive control and the TA. It should be noted that, although the TA showed an inhibition percentage of 100%, an inhibition phenomenon caused by the acidic properties of the compound occurred. The TA solution has a pH of 3.5, hence upon contact with the culture medium, the proteins of this will precipitate so that they will not be bioavailable for bacteria causing disadvantages from the beginning for bacterial growth (Bhattacharya 2019). On the other hand, Zn-LHS particles are unstable and precipitate out. TA adsorbed on top LHS favored the colloidal nature of the compound, maintaining appropriate conditions for bacterial growth allowing the quantification the inhibition of percentage by the action of the TA-Zn-LHS complex.

The concentration and species form of Zn influences the antimicrobial activity, the mechanisms of action of these compounds, depending on their soluble and insoluble forms is describe by Abendrot and Kalinowska-Lis (2018). In the case of soluble Zn compounds, an interaction between Zn^{2+} ions and the cell membrane is proposed, generating a destabilization and permeability of the cell membrane. In the case of insoluble compounds and ZnO compounds, the production of reactive oxygen species (ROS), the direct destruction of the cell wall by coming into direct contact with the microbial cell membrane and the cytotoxic effect triggered by the release of Zn^{2+} ions are proposed. The recent use of TA as a base forming polyphenolic metal networks has been extended to the elaboration of metal–organic matrices fabricated using metal ions and organic molecules. The adjacent OH groups of tannic acid react with different metal ions by coordinating and providing chelating sites. The steric hindrance provided by the aromatic rings and the electron donating/accepting interaction between adjacent phenolic groups gives molecular stability to the nanoparticles allowing the participation of tannic acid in biological processes through functional metal chelation (Chen et al. 2022).

The inhibition mechanism of tannic acid has been related to the direct binding of the molecule to the peptidoglycan layer in the cell wall, interfering with its integrity and generating an antimicrobial effect. In addition, it also participates inhibiting biofilm formation in Gram-positive bacteria (Xu et al. 2019). As shown in Fig. 3, TA-Zn-LHS evidenced statistically significantly lower inhibition with 87.48%, 75.23% and 88.75% antibiofilm activity on *E. coli* ATCC 8739 (Fig. 3a), *S.* Enteritidis (Fig. 3b) and *S. aureus* ATCC 25923 (Fig. 3c), respectively, contrary to the > 90% BFI shown by Zn-LHS. BFI by Zn-LHS has also been reported for *P. aeruginosa* by Velázquez-Carriles et al. (2022) with 89% at 10 mg /mL concentration. This study revealed an increase in the antibiofilm activity with respect to an increase in concentration, as well as the inclusion of bioactive compounds such as thymol in its structure, indicating the specific interaction

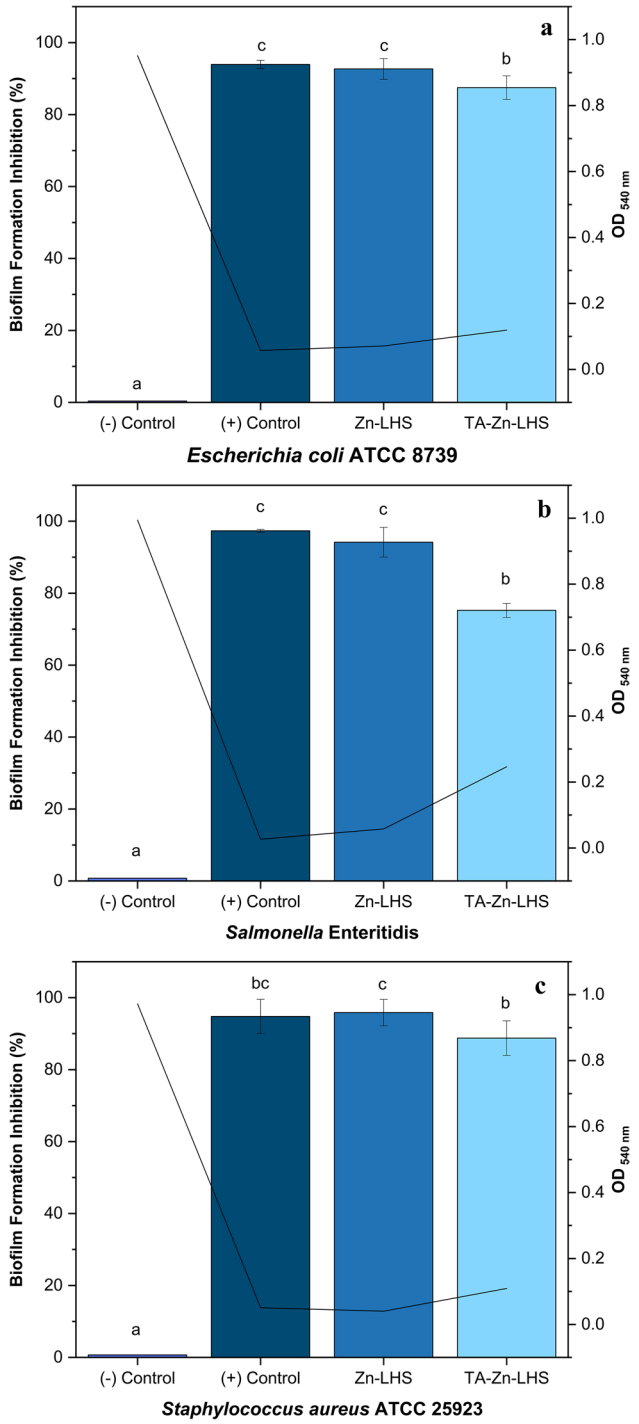

Fig.3 Biofilm inhibition activity to: **a** *Escherichia coli* ATCC 8739; **b** *Salmonella* Enteritidis; **c** *Staphylococcus aureus* ATCC 25923. (−) Control: Strain inoculum; (+) Control: 0.1 mg/mL Ampicillin; OD: Optical Density. Different letters show statistical significance differences ($p < 0.05$) by Tukey's test

between the bacterial membrane with the nanohydroxide with hydrophobic character.

Table 2 Antioxidant capacity of zinc nanohydroxide and TA nanohybrid

Material	DPPH (μM EqTA)	ABTS (μM EqTA)	FRAP (μM EqTA)
Zn-LHS	N.D	N.D	0.56 ± 0.06
TA-Zn-LHS	9.61 ± 0.92	20.72 ± 0.77	33.52 ± 7.60

DPPH 2,2 diphenyl-1-picrylhydrazyl, *ABTS* 2,2′-azino-bis(3-ethylbenzothiazoline-6-sulfonate), *FRAP* Ferric reducing antioxidant power, *μM EqTA* μM equivalents of tannic acid. *N.D.* Not determinable

Since we could observe that the layered hydroxides in which tannic acid was not incorporated also showed inhibition against the bacterial strains, it is essential to highlight those properties that could influence the inhibition mechanism. Cell membranes present a negative charge, which should be considered for the use of nanoparticles with potential antimicrobial activity. Because the ζ of these materials can affect permeability in bacterial cells, disrupting the cell wall thus inhibiting bacterial growth. Baig et al. (2022), highlight the antimicrobial effect of Simonkolleite/Zn nanostructures with evident antimicrobial and antifungal activity on human pathogens. The authors propose an inhibition mechanism in which Zn nanoparticles promote the generation of free radicals permeating the membrane and nano-inducing cell death.

Antioxidant evaluation of TA-Zn-LHS

The DPPH and ABTS antioxidant capacity and the ferric reducing antioxidant power of the nanohybrid with TA are summarized in Table 2. The results presented for the antioxidant activity DPPH and ABTS confirmed the presence of TA in Zn-LHS by showing a higher percentage of inhibition of the radicals (17.21% and 82.02%, respectively; data not shown) than Zn-LHS, in which it was not determinable at 1 mg Zn-LHS / mL distilled water. The measurements performed for ABTS showed antioxidant activity of 20.72 μM EqTA, greater than the 9.61 μM EqTA for DPPH assay. In determining the ferric reducing antioxidant potential, higher activity was observed in the TA nanohybrid with 33.52 μM EqTA, in contrast with the 0.56 μM EqTA of the Zn-LHS. The antioxidant activity of the tannic acid compound has been reported to show scavenging properties for reactive oxygen species, evidencing its DPPH antioxidant activity (Gülcin et al. 2010). This behavior, observed in other nanoparticles in which the antioxidant activity is preserved, is expected in nanohybrids (Pucci et al. 2022); the effectiveness of the antioxidant activity of TA in the inorganic matrix is stablished by the interaction of the free active sites of the compound present in the TA-Zn-LHS complex. On the other

Table 3 Toxicity activity to *Artemia salina* brine shrimp

Material	µg/mL	Mortality (%)	Degree of toxicity
Tannic acid	600	33.33	ST
	60	26.67	ST
	6	3.33	NT
Zn-LHS	1000	16.67	ST
	100	16.67	ST
	10	0.00	NT
TA-Zn-LHS	1000	43.33	ST
	100	26.67	ST
	10	3.30	NT

ST Slightly toxic, *NT* Non-toxic

hand, FRAP activity performs adsorption and neutralization of free radicals due to its redox potential. Consequently, the presence of high FRAP values indicates a higher antioxidant capacity due to the reduction of ferric ions, allowing the determination of total antioxidant levels Raajshree and Durairaj (2017).

Toxicity of Zn-LHS and TA-Zn-LHS to *Artemia salina* brine shrimp

Considering the vital antimicrobial and antioxidant effect found in nanohydroxides with and without TA, it is crucial to evaluate the toxicity these materials may have to if apply in the food industry. The evaluation to toxicity in *A. salina* is summarized in Table 3. The negative toxicity control (artificial seawater, not shown in the table) was found to have 0% mortality, classifying the experimental conditions as non-toxic (NT). On the other hand, the positive death control DMSO (not shown in the table) exhibited 40% mortality and was considered slightly toxic (ST) according to the toxicity criteria. As summarized in Table 3, both TA and the nanohydroxides evidenced toxicity from NT to ST from the lowest to the highest concentration evaluated, corresponding to the estimated concentration of the bioactive compound in the nanohybrids. This behavior has been observed in Zn and ZnO nanoparticles in the same biological model where a dose- and time-dependent toxicity relationship was demonstrated, presenting higher toxicity at higher concentrations and 24 h exposure. In addition, the presence of smaller Zn-nanoparticles (40–60 and 80–100 nm) than those present in this study (400–500 nm) generates a bioaccumulation phenomenon in *A. salina* resulting in more significant toxicity (Dannabas et al. 2020). These results presume an inorganic matrix with biological functions without generating an adverse effect concerning its safe use in the food or food packaging industry.

Conclusions

In concluding remarks, this study succeeded in synthesizing a hybrid zinc nanohydroxide with tannic acid. The adsorption of TA was evidenced by XRD patterns, FT-IR spectra, and its hydrodynamic properties. In addition, a change in the crystalline surface structure of Zn-LHS in the presence of TA was observed, presuming an interfacial concentration of 0.64 mg of TA per mg of Zn-LHS according to UV–vis analysis. The synthesized material, TA-Zn-LHS, exhibited antimicrobial and antibiofilm activity against Gram-positive and Gram-negative foodborne pathogens. In addition, the preservation of DPPH, ABTS and FRAP antioxidant activity of TA was corroborated and is higher than that of Zn-LHS. The classification of the materials as non-toxic to slightly toxic, allows to propose the nanohybrid with TA as a safe material for use in the food industry.

Acknowledgements The authors thank Dra. María Esther Macías-Rodríguez for the donation of *Salmonella* Enteritidis and the support of the Molecular Biology Laboratory; and Sarahi Ipiña López for technical assistance in the antimicrobial activity experiments.

Author contributions RGDM conducted the experimental research, analyzed the data, and wrote the original draft. GC and VCCA performed the design of experiments, analyzed the data, reviewed drafts of this paper, and proofread the language. SJJM provided resources and performed the design of experiments, analyzed the data, and wrote the original draft. VJG supported and reviewed the antioxidant activity experiments and reviewed draft of this paper.

Funding RGDM wants to thank CONACyT (Consejo Nacional de Ciencia y Tecnología) for the financial support provided through the doctoral grant (No. 973558). The authors also thank COECYTJAL (Consejo Estatal de Ciencia y Tecnología) for the financial support of some material through the project FODECIJAL 8122–2019.

Data availability The data supporting this research is available upon reasonable request to the corresponding author's email address.

Code availability Not applicable.

Declarations

Conflict of interest All authors declare no conflict of interest.

Ethical approval Authors approve the ethical requirements.

Consent to participate All authors endorsed the consent statements.

Consent for publication All authors approved the consent for publication in the Journal of Food Science and Technology.

References

Abendrot M, Kalinowska-Lis U (2018) Zinc-containing compounds for personal care applications. Int J Cosmet Sci 40(4):319–327. https://doi.org/10.1111/ics.12463

Baig MM, Hassan M, Ali T, Asif HM, Asghar A, Ullah S, Alsafari IA, Zulfiqar S (2022) Green 2D simonkolleite/zinc based nanostructures for superior antimicrobial and photocatalytic applications. Mater Chem Phys 287:126292. https://doi.org/10.1016/j.matchemphys.2022.126292

Balouiri M, Sadiki M, Ibnsouda SK (2016) Methods for in vitro evaluating antimicrobial activity: a review. J Pharm Anal 6(2):71–79. https://doi.org/10.1016/j.jpha.2015.11.005

Benzie IF, Strain JJ (1996) The ferric reducing ability of plasma (FRAP) as a measure of "antioxidant power": the FRAP assay. Anal Biochem 239:70–76. https://doi.org/10.1006/abio.1996.0292

Bhattacharya A (2019) High-temperature stress and metabolism of secondary metabolites in plants. Effect of high temperature on crop productivity and metabolism of macro molecules. Elsevier, pp 391–484. https://doi.org/10.1016/B978-0-12-817562-0.00005-7

Bouaziz Z, Soussan L, Janot JM, Jaber M, Ben Haj Amara A, Balme S (2018) Dual role of layered double hydroxide nanocomposites on antibacterial activity and degradation of tetracycline and oxytetracyline. Chemosphere 206:175–183. https://doi.org/10.1016/j.chemosphere.2018.05.003

Brand-Williams W, Cuvelier ME, Berset C (1995) Use of a free radical method to evaluate antioxidant activity. Food Sci Technol 28(1):25–30. https://doi.org/10.1016/S0023-6438(95)80008-5

Carbajal-Arízaga GG, Satyanarayana K, Wypych F (2007) Layered hydroxide salts: synthesis, properties and potential applications. Solid State Ion 178(15–18):1143–1162. https://doi.org/10.1016/j.ssi.2007.04.016

Casas-Junco PP, Solís-Pacheco JR, Ragazzo-Sánchez JA, Aguilar-Uscanga BR, Bautista-Rosales PU, Calderón-Santoyo M (2019) Cold plasma treatment as an alternative for ochratoxin a detoxification and inhibition of mycotoxigenic fungi in roasted coffee. Toxins 11(6):337. https://doi.org/10.3390/toxins11060337

Chen C, Yang H, Yang X, Ma Q (2022) Tannic acid: a crosslinker leading to versatile functional polymeric networks: a review. RSC Adv 12(13):7689–7711. https://doi.org/10.1039/d1ra07657d

Danabas D, Ates M, Tastan BE, Cimen ICC, UnalI AO, Kutlu B (2020) Effects on Zn and ZnO nanoparticles on *Artemia salina* and *Daphnia magna* organisms: toxicity, accumulation and elimination. Sci Total Environ 711:134869. https://doi.org/10.1016/j.scitotenv.2019.134869

Gülçin İ, Huyut Z, Elmastaş M, Aboul-Enein HY (2010) Radical scavenging and antioxidant activity of tannic acid. Arab J Chem 3(1):43–53. https://doi.org/10.1016/j.arabjc.2009.12.008

Kaczmarek B (2020) Tannic acid with antiviral and antibacterial activity as a promising component of biomaterials-a minireview. Materials. https://doi.org/10.3390/ma13143224

Lancheros RJ, Beleño JÁ, Guerrero CA, Godoy-Silva RD (2014) Producción de nanopartículas de plga por el método de emulsión y evaporación para encapsular N-acetilcisteína (NAC). Univ Sci 19(2):161–168. https://doi.org/10.11144/Javeriana.SC19-2.pnpm

Li H, Wang X, Li Y, Li P, Wang H (2009) Polyphenolic compounds and antioxidant properties of selected China wines. Food Chem 112(2):454–460. https://doi.org/10.1016/j.foodchem.2008.05.111

Mohsin SMN, Hussein MZ, Sarijo SH, Fakurazi S, Arulselvan P, Hin TYY (2013) Synthesis of (cinnamate-zinc layered hydroxide) intercalation compound for sunscreen application. Chem Cen J 7(1):1–12. https://doi.org/10.1186/1752-153X-7-26

Nakagaki S, Machado GS, Stival JF, Henrique dos Santos E, Silva GM, Wypych F (2021) Natural and synthetic layered hydroxide salts (LHS): recent advances and application perspectives emphasizing catalysis. Prog Solid State Ch 64:100335. https://doi.org/10.1016/j.progsolidstchem.2021.100335

O'Toole GA (2011) Microtiter dish biofilm formation assay. J vis Exp. https://doi.org/10.3791/2437

Orlowski P, Zmigrodzka M, Tomaszewska E, Ranoszek-Soliwoda K, Czupryn M, Antos-Bielska M, Szemraj J, Celichowski G, Grobelny J, Krzyzowska M (2018) Tannic acid-modified silver nanoparticles for wound healing: the importance of size. Int J Nanomedicine 13:991–1007. https://doi.org/10.2147/IJN.S154797

Pucci C, Martinelli C, De Pasquale D, Battaglini M, di Leo N, Degl'Innocenti A, Ciofani G, (2022) Tannic Acid–iron complex-based nanoparticles as a novel tool against oxidative stress. ACS Appl Mater Interfaces 14(14):15927–21594. https://doi.org/10.1021/acsami.1c24576

Raajshree KR, Durairaj B (2017) Evaluation of the antityrosinase and antioxidant potential of zinc oxide nanoparticles synthesized from the brown seaweed–turbinaria conoides. Int J Appl Pharm 9(5):116–120. https://doi.org/10.22159/ijap.2017v9i5.20847

Rezaei A, Fathi M, Jafari SM (2019) Nanoencapsulation of hydrophobic and low-soluble food bioactive compounds within different nanocarriers. Food Hydrocoll 88:146–162. https://doi.org/10.1016/j.foodhyd.2018.10.003

Sánchez-Maldonado AF, Lee A, Farber JM (2018) Methods for the control of foodborne pathogens in low-moisture foods. Annu Rev Food Sci Technol 9(1):177–208. https://doi.org/10.1146/annurev-food-030117-012304

Santos AFM, Macedo LJA, Chaves MH, Espinoza-Castañeda M, Merkoçi A, Limac FDCA, Cantanhêde W (2016) Hybrid self-assembled materials constituted by ferromagnetic nanoparticles and tannic acid: a theoretical and experimental investigation. J Braz Chem Soc 27(4):727–734. https://doi.org/10.5935/0103-5053.20150322

Srivastava OK, Secco EA (1967) Studies on metal hydroxy compounds. Infrared spectra of zinc derivatives ε-Zn (OH) 2, β-ZnOHCl, ZnOHF, Zn_5 (OH) $8Cl_2$, and Zn_5 (OH) $8Cl_2H_2O$. Can J Chem 45(6):585–588. https://doi.org/10.1139/v67-097

Velázquez-Carriles CA, Carbajal-Arízaga GG, Silva-Jara JM, Reyes-Becerril MC, Aguilar-Uscanga BR, Macías-Rodríguez ME (2020) Chemical and biological protection of food grade nisin through their partial intercalation in laminar hydroxide salts. J Food Sci Technol 57(9):3252–3258. https://doi.org/10.1007/s13197-020-04356-y

Velázquez-Carriles C, Macías-Rodríguez ME, Ramírez-Alvarado O, Corona-González RI, Macías-Lamas A, García-Vera I, Silva-Jara JM (2022) Nanohybrid of thymol and 2D simonkolleite enhances inhibition of bacterial growth, biofilm formation, and free radicals. Molecules 27(19):6161. https://doi.org/10.3390/molecules27196161

Wahyono T, Astuti DA, Komang Gede Wiryawan I, Sugoro I, Jayanegara A (2019) Fourier transform mid-infrared (FTIR) spectroscopy to identify tannin compounds in the panicle of sorghum mutant lines. IOP Conf Ser Mater Sci Eng. https://doi.org/10.1088/1757-899X/546/4/042045

World Health Organization (2015) WHO estimates of the global burden of foodborne diseases: foodborne disease burden epidemiology reference group 2007–2015. World Health Organization. https://apps.who.int/iris/bitstream/handle/10665/199350/?sequence=1. Accessed 23 Nov 2022

Xu D, Hu MJ, Wang YQ, Cui YL (2019) Antioxidant activities of quercetin and its complexes for medicinal application. Molecules 24(6):1123. https://doi.org/10.3390/molecules24061123